Metal–Organic Framework Mediated Cobalt/Nitrogen-Doped Carbon Hybrids as Efficient and Chemoselective Catalysts for the Hydrogenation of Nitroarenes

Sun, Xiaohui; Olivos-Suarez, Alma I.; Oar-Arteta Gonzalez, L.; Rozhko, Elena; Osadchii, Dmitrii; Bavykina, Anastasiya; Kapteijn, Freek; Gascon, Jorge

DOI
10.1002/cctc.201700095

Publication date
2017

Document Version
Accepted author manuscript

Published in
ChemCatChem

Citation (APA)
Sun, X., Olivos-Suarez, A. I., Oar-Arteta Gonzalez, L., Rozhko, E., Osadchii, D., Bavykina, A., Kapteijn, F., & Gascon, J. (2017). Metal–Organic Framework Mediated Cobalt/Nitrogen-Doped Carbon Hybrids as Efficient and Chemoselective Catalysts for the Hydrogenation of Nitroarenes. *ChemCatChem*, *9*(10), 1854-1862. https://doi.org/10.1002/cctc.201700095

Metal-Organic-Framework Mediated Cobalt/N-Doped Carbon Hybrids as Efficient and Chemoselective Catalysts for the Hydrogenation of Nitroarenes

Xiaohui Sun, Alma I. Olivos-Suarez, Lide Oar-Arteta, Elena Rozhko, Dmitrii Osadchii, Anastasiya Bavykina, Freek Kapteijn, and Jorge Gascon*

Abstract: A Co@N-doped carbon (Co@NC) hybrid was synthesised *via* thermal decomposition of the metal organic framework (MOF) ZIF-67 under N_2 atmosphere. These hybrid materials exhibit outstanding catalytic activity and chemoselectivity for the conversion of a wide range of substituted nitroarenes to their corresponding anilines under relatively mild reaction conditions. The high catalytic performance is attributed to the formation of cobalt nanoparticles and to the presence of atomically dispersed Co species in close interaction with nitrogen doped graphene. Both active species are formed *in situ* during the pyrolytic transformation of ZIF-67. The catalysts could be reused in consecutive runs, exhibiting a slightly lower activity ascribed to blockage of the active sites by strongly adsorbed reaction species. These results open up a pathway for the design of noble-metal free solid catalysts for industrial applications.

Introduction

Anilines and, in particular their functionalised derivatives, are key organic intermediates for manufacturing dyes, pharmaceuticals, pigments, and agrochemicals obtained *via* reduction of their corresponding nitroarenes.[1] Conventional Béchamp (using Fe/HCl) or sulfide reduction (with H_2S or NaSH as reducing agents) processes are widely applied to produce functionalised anilines in industry.[2] However, these non-catalytic processes generate large amounts of undesirable waste, resulting in severe environmental problems. Because of these reasons, the direct catalytic hydrogenation of nitroarenes has been extensively studied over the last few years.[3]

In this spirit, a large number of molecular catalysts have been developed.[4] However, these homogeneous catalysts suffer from difficulties in recycling and separation from products. Therefore, heterogeneous catalysts consisting of supported metal nanoparticles (NPs) are more attractive. Supported Pt catalysts have been proposed as alternative and are used in the direct hydrogenation of nitroarenes.[5] However, despite very efficient for the activation of nitro groups, Pt is also an excellent catalyst for the reduction of carbonyl groups and double bonds, which usually leads to unselective hydrogenations.[6] An alternative to improve the chemoselectivity of supported Pt catalysts is to introduce additives, such as PdO or H_3PO_2, *albeit* in most cases at the expense of activity.[6-7] Lack of selective hydrogenation is not the only associated problem. Side products such as phenylhydroxylamine derivatives, one type of byproduct formed with Pt-PbO or Pt-H_3PO_2 catalysts during the hydrogenation process, can be explosive even at low concentrations.[6a] Recently, Corma *et. al* investigated this reaction using gold instead of platinum. This less active hydrogenation metal surprisingly exhibited high activity and chemoselectivity to the corresponding substituted anilines.[3b, 8] Along with the use of Au, recent efforts have led to the development of cheaper first-row transition metal-based hydrogenation catalysts (*e.g.* Fe, Co and Ni).[1a, 9] However, most of these supported noble metal-free catalysts are not yet ideal because of lack of stability, activity and in some cases reusability. Major problems are aggregation, metal leaching and/or metal surface modification under reaction conditions.[9-10]

Different strategies have been proposed to improve the stability of metal nanoparticles, including coating with organic molecules, polymers or oxides.[11] For instance, cobalt NPs were reported to be protected against agglomeration and air oxidation by capping with organic ligands. In general, these coatings possess poor electron conductivity and can effectively block charge transfer between catalytic site and reagents, thereby negatively influencing the catalytic activity. In contrast, graphite-like carbon coatings with unique chemical, electrical, and functional properties are capable of protecting transition metal (*e.g.* Co, Fe) NPs from agglomeration and re-oxidation by air,[12] while preserving high activities in a variety of catalytic reactions.[12-13] Recently, the group of Beller developed a novel heterogeneous catalyst in which cobalt nanoparticles are embedded in a N-doped carbon matrix *via* direct carbonization of non-volatile Co-amine coordination complexes.[3a] This cobalt/N-doped carbon hybrid shows outstanding activity in the hydrogenation of different nitroarenes along with chemoselectivity to their substituted anilines. Although cobalt is claimed to play a crucial role in this system, the reasons behind such high activity still remain elusive, largely because of the complexity of the system. Cheng *et al.* suggested that those exposed cobalt nanoparticles does not play a role in the hydrogenation activity, and proposed that the real active sites are highly dispersed Co-N_x species located at the carbon matrix.[14] However, Liu *et al.* indicated no detectable hydrogenation activity after acid leaching in a Co@C catalyst, and concluded that the hydrogenation activity is to be attributed to those accessible metallic cobalt NPs.[15] Similarly, Wang *et al.* neither detected any hydrogenation activity after leaching Co with aqua regia on a Co@NC catalyst using ZIF-67 as template.[16] On the other hand, along the already mentioned issues in the identification of the active sites in Co-based catalysts, recycling is also confronted with great challenges. Indeed, most of these cobalt-based catalysts deactivate in a couple of runs. Chen *et al.* observed the gradual oxidation of cobalt in Co@C during the hydrogenation process.[17] However, Wei and Liu both claimed that oxidized cobalt can be *in situ* reduced to its metallic phase by H_2 under hydrogenation conditions.[9a, 15]

In order to further contribute to this discussion, we prepared N-doped Co@NC composites *via* one-step pyrolysis of ZIF-67 in a N_2 atmosphere along with an in-depth investigation on the nature of the active sites and the reasons behind deactivation during the hydrogenation of different nitroarenes. We

demonstrate that the pyrolysis temperature and heterogeneity of metal species play a major role in the challenging hydrogenation of nitroarenes over Co based catalysts.

Results and Discussion

Catalyst Characterization Results

ZIF-67 was synthesised by mixing a cobalt nitrate methanolic solution and MeIm at room temperature. The relative intensity and peak positions of the powder X-ray diffraction (PXRD) pattern confirm the formation of pure crystalline ZIF-67 (Figure S1a).[18] Thermogravimetric (TG) analysis of the synthesized ZIF-67 under N_2 atmosphere suggests that ZIF-67 crystals are thermally stable up to 480 °C (Figure S1b). The sample weight then decreases sharply along with temperature increase until 600 °C, which can be ascribed to the decomposition of the organic linker (MeIm).[19] After that, the sample weight decline slows down steadily up to 800 °C, implying that the majority of organic fraction has decomposed below 600 °C.

The specific BET area (S_{BET}) and pore volume (V_{pore}) of ZIF-67 and Co@NC-*T* samples were determined by N_2 adsorption-desorption isotherms (Table S1 and Figure S2). ZIF-67 with a high S_{BET} of 1930 m^2 g^{-1}, displays a type I isotherm with a steep N_2 uptake at low relative pressures, typically associated with microporosity.[20] After pyrolysis at 600 °C, the S_{BET} of Co@NC-*600* drastically decreases to ~400 m^2 g^{-1}, due to the collapse of the well-defined microporous structure of ZIF-67 during the carbonization process (note that this area is referred to the support, as explained above).[19a, 21] A hysteresis loop also appears with gradual N_2 uptake at a relative pressure from 0.45 to 1.0, caused by the capillary condensation of N_2 in mesopores with a wide size distribution. The microporous volume of Co@NC-*600* is considerably smaller (0.1 cm^3 g^{-1}) compared to the parent ZIF-67 (0.68 cm^3 g^{-1}). In contrast, an increase in mesoporous volume for the pyrolyzed sample from 0.03 cm^3 g^{-1} to 0.14 cm^3 g^{-1} is also observed. The pore structure change proves that the original microporosity of ZIF-67 was transformed into an hierarchically interconnected micro/mesoporous structure during the pyrolysis process. Interestingly, further rising of the pyrolysis temperature does not significantly influence the S_{BET} and V_{pore} of Co@NC. Although the overall S_{BET} and V_{pore} do

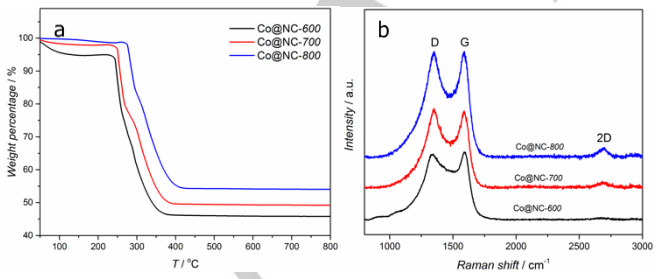

Figure 1. (a) TGA profile of Co@NC-*T* under air flow (100 ml min^{-1} STP, heating rate 5 K min-1), (b) Raman spectra of Co@NC-*T*.

decrease due to the lower amount of support after different pyrolysis temperatures, the structure of the support does not change, as inferred by the similar S_{BET} and V_{pore} values obtained per gram of support.

Figure 1a shows the thermogravimetric (TG) analyses under air atmosphere of the Co@NC-*T* samples. All samples present approximately the same oxidation profile. There are two major mass losses directly attributed to two carbonaceous species bearing different thermal stabilities.[22] Despite these similar profiles, the final residual mass, attributed to Co_3O_4, increases with pyrolysis temperature, related to the fact that the carbon content decreases with pyrolysis temperature. According to AAS (atomic adsorption spectroscopy) analysis, the Co concentrations in Co@NC-*T* catalysts are 31.0 *wt.*% 32.9 *wt.*% and 37.4 *wt.*% for Co@NC-*600*, *-700*, and *-800*, respectively (Table S2). More importantly, the pyrolysis temperature also impacts the initial oxidation temperature of the carbon matrix in Co@NC-*T* samples. The higher the pyrolysis temperature used, the higher the temperature for carbon oxidation, pointing out to a higher graphitization degree of the carbon structure. This can be also inferred from the Raman spectra in Figure 1b. All the Raman spectra of Co@NC-*T* reveal the characteristic G and D bands of carbon at 1580 cm^{-1} and 1350 cm^{-1}, which are correlated to graphitic sp^2-carbon and disordered or defect carbon, respectively.[23] When a higher pyrolysis temperature is employed (*i.e.* 700 °C), a new band around 2700 cm^{-1} appears and sharpens with further increasing pyrolysis temperature to 800 °C. This signal can be assigned to the 2D band of graphitic carbon.[19a, 24]

The TEM images of Co@NC-*T* in Figure 2a-c indicate that cobalt NPs are uniformly dispersed in the N-doped carbon matrix. The average particle size of Co NPs in Co@NC-*T* is dependent on the pyrolysis temperature (°C), increasing from 8 nm in '*-600*' to 12 nm and 18 nm for '*-700*' and '*-800*', respectively (Figure 2d-f). Clearly, higher pyrolysis temperatures induce aggregation of Co to larger NPs.[19a] The high-resolution (HR) TEM image of Co@NC-*T* (see insert in Figure 2a-c) reveals a lattice fringe of 2.05 Å attributed to the (111) plane of Co^0, and confirms that the Co^0 NP is embedded in N-doped carbon matrix and encapsulated by a few graphitic-like carbon layers, inferring a highly stable catalytic system.[12b] In view of these results, it can be proposed that Co^{2+} in the structure of ZIF-67 is reduced during the pyrolysis process to Co^0, and that the final size of the formed Co nanoparticles can be controlled by varying the pyrolysis temperature. At the same time, these NPs facilitate the formation of graphitic carbon layers surrounding the nanocrystals during the pyrolysis and cooling down period.[25]

The presence of Co^0 and crystalline carbon is also observed in the XRD patterns shown in Figure 3a. All Co@NC samples exhibit a diffraction peak at 30.6°, indexed to the (002) planes of graphitic carbon (JCPDS No. 75-1621)[26]. In addition, the two peaks at 51.8° and 60.6° indicate the diffraction of the (111) and (200) planes of metallic cobalt, respectively (JCPDS No. 15-0806)[27]. The diffraction peaks of both graphite and Co^0 become narrower and sharper as the pyrolysis temperature increases, pointing to a higher graphitization degree of the carbon matrix

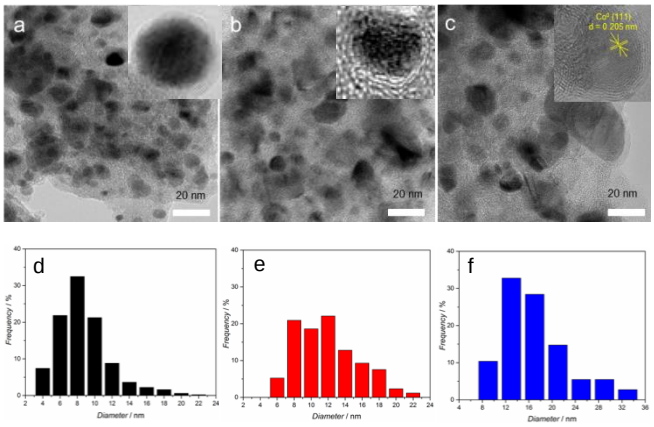

Figure 2. TEM images and corresponding size distribution of Co NPs in Co@NC-*T*: (a, d) 600 °C, (b, e) 700 °C, (c, f) 800 °C.

and to the formation of larger cobalt NPs. Importantly, no cobalt oxide and/or cobalt carbide reflections are found.

X-ray photoelectron spectroscopy (XPS) was further employed for all Co@NC-*T* samples to analyse the bonding state of nitrogen, as stated in Figure 3b. N *1s* signals of Co@NC-*T* were deconvoluted into three types of nitrogen species with binding energies around 398.8 eV, 400.8 eV, and 402.3 eV, which can be attributed to pyridinic-N, graphitic-N (pyrrolic and quaternary–N) and oxidized-N,[23, 28] respectively. The peak at a binding energy of 398.8 eV could also be partially due to a contribution from nitrogen bound to the metal (Me-N), due to the small difference between binding energies of N-Me and pyridinic N.[29] Evidently, the N atoms in the pentagonal ring of the original imidazole units were mostly converted into two types of N moieties (pyridinic- and graphitic-N) during the carbonization process. The pyridinic-N to graphitic-N atomic ratio (Table S3) decreases from 3.3 for '*-600*' to 2.4 for '*-700*' and 1.3 for '*-800*', demonstrating that relatively more nitrogen atoms incorporate into the graphitic carbon layers at higher pyrolysis temperatures. According to elemental analysis, the N contents in the three catalysts are 7.8 *wt.*% for Co@NC-*600*, 3.7 *wt.*% for Co@NC-*700*, and 2.4 *wt.*% for Co@NC-*800* (Table S2), indicating a loss of nitrogen with increasing thermal decomposition temperature.[3c, 28]

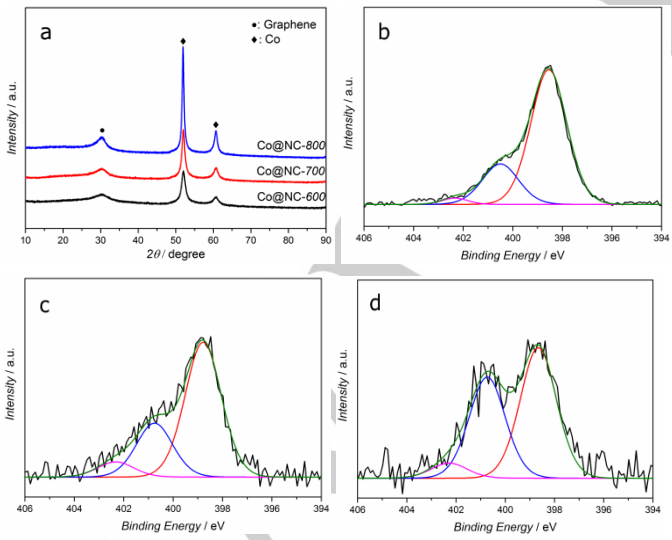

Figure 3. (a) XRD patterns of Co@NC-*T*, N *1s* XPS region of (b) Co@NC-*600*, (c) Co@NC-*700*, (d) Co@NC-*800*.

Catalytic Performance in Nitrobenzene Hydrogenation.

The catalytic activity of the Co@NC-*T* materials was assessed in the hydrogenation of nitrobenzene (Table 1). In order to clearly understand the catalytic activity of the Co@NC-*T* materials, a series of control experiments were performed. Neither blank runs (without catalyst) nor the parent ZIF-67 (Table 1, entries 1, 2) showed any conversion, indicating that the active species should be formed during the pyrolysis process. Furthermore, the comparable NC sample[30] synthesised using ZIF-8(Zn) as precursor (Figure S1c) exhibited no activity (Table 1, entry 13), whereas the as-synthesized Co@NC-*T* catalysts exhibit good hydrogenation activity together with a >99% selectivity to aniline, suggesting that cobalt-containing species are responsible for the catalytic action in this reaction. More interestingly, the hydrogenation activity of these Co@NC-*T* catalysts (Table 1, entries 3-5) correlates with the pyrolysis temperature, with conversions after 3 h reaction ranging from 48% to 69% as the pyrolysis temperature increases from 600 to 800 °C (note that the amount of Co used in all cases was similar). Given that the S_{BET} and V_{pore} of Co@NC do not vary with pyrolysis temperature (Table S1), the different hydrogenation activity for these Co@NC has to be attributed to: (i) the different feature of the N-doped carbon matrix, such as the graphitization degree, that might have an impact on hydrogen dissociation;[31] (ii) the cobalt speciation or particle size. The impact of reaction temperature on the catalytic activity for Co@NC-*800* further shows that the conversion of nitrobenzene is below 15% for a reaction temperature below 70 °C (Table S4). However, the activity sharply rises with the reaction temperature, and reaches 99% conversion after 3 h at a reaction temperature of 110 °C. Moreover, similar turnover numbers (*TON*s) are obtained for experiments performed with different initial concentrations of nitrobenzene on Co@NC-*800* (Table S5), indicating an apparent zeroth order reaction with respect to this reactant, attributed to a strong adsorption of nitrobenzene on the catalyst in these experiments.

The Co@NC-*T* catalysts were further post-treated in a 0.5 M HCl solution to remove those accessible cobalt NPs (hence, acid leached samples are denoted as Co@NC-*T (al)*). AAS analysis indicates that cobalt content in the acid leached samples is 27.1 *wt.*% for Co@NC-*600 (al)*, decreasing to 4.1 *wt.*% for Co@NC-*900 (al)*, (Table S2). Apparently, a larger fraction of cobalt can be leached out by acid when ZIF-67 is carbonized at a higher temperature. At the same time, XRD analysis (Figure S3 and Table S6) clearly demonstrates that these acid leached Co@NC-*T (al)* samples still contain metallic cobalt nano-

Table 1. Results of the catalytic hydrogenation of nitrobenzene over Co@NC-*T* and Co@NC-*T* (*al*).[a]

Entry	Catalyst	Co content (wt. %)	Substrate to cobalt molar ratio	*X* (%)[b]	*TON*[c]
1	Blank	-	-	< 1	-
2	ZIF-67	26.0	37	< 1	-
3	Co@NC-*600*	31.0	37	48	18
4	Co@NC-*700*	32.9	37	57	21
5	Co@NC-*800*	37.4	37	69	24
6	Co@NC-*800*	37.4	24	99	24
7	Co@NC-*700*	32.9	35	59	21
8	Co@NC-*800*	37.4	31	79	24
9	Co@NC-*600 (al)*	27.1	43	43	18
10	Co@NC-*700 (al)*	19.4	60	38	22
11	Co@NC-*800 (al)*	13.6	85	62	53
12[d]	Co@NC-*800 (al)*	13.6	85	39	33
13	NC-*800 (al)*	-	-	< 1	-
14	Co@NC-*900 (al)*	4.1	282	36	101

[a] Reaction conditions: 1 mmol nitrobenzene, 5 mL ethanol, 110 °C, 3 MPa H_2, 3 h, aniline selectivity in all cases > 99% (no byproducts were detected by GC analysis, carbon balance nears 100% in all cases). [b] Determined by GC (internal standard: *n*-hexadecane), *X* = mol nitrobenzene consumed divided by total mol nitrobenzene. [c] *TON* = mol nitrobenzene consumed divided by total mol cobalt. [d] 0.02 M NaSCN as catalyst inhibitor with SCN^- to cobalt molar ratio of 8.5.

particles with a similar average Co particle size. These Co nanoparticles exhibit high resistance toward acid leaching, owing to a well encapsulation by graphitic carbon layers on the surface.[32] As it is well known, acid leaching under mild conditions is only able to remove those Co nanoparticles that are not fully encapsulated by the graphite shells.[33] Hydrogenation experiments were further performed with these leached samples using a similar total amount of catalyst (5.1 mg) of Co@NC-*T (al)* and Co@NC-*T* (Table 1, entry 3, 7-11,14). Obviously, the Co@NC-*T (al)* samples exhibit a lower nitrobenzene conversion compared to their counterparts, *albeit* with similar aniline selectivity, suggesting that those leached cobalt nanoparticles did participate in the hydrogenation reaction. Interestingly, the Co@NC-*T (al)* samples (*T* = 600, 700, 800 °C) still retain a considerable activity and Co@NC-*800 (al)* exhibits the highest nitrobenzene conversion (62%) among the three Co@NC-*T (al)* samples, indicating that acid-leaching resistant cobalt species are able to perform the hydrogenation as well.

Recently, Wang *et al.*, reported a similar strategy to prepare Co@NC catalyst by pyrolysis of ZIF-67, and claimed that no hydrogenation activity was observed after acid leaching in aqua regia.[16] Bearing in mind the superior oxidation capacity of aqua regia, this is not surprising. Indeed, it has been reported by other authors that N-doped graphene can be easily destroyed by acid treatment in concentrated HNO_3, one of the main components of aqua regia.[14] In order to gain more insight into the nature of the active sites in our Co@NC-*800 (al)*, a series of characterization measurements were performed. The Raman and C *1s* XPS spectra of Co@NC-*800 (al)* (Figure S4 and Figure S5a,b) are similar to those of the non-acid leached sample, suggesting that a possible carbon surface modification is not responsible for a change in activity. Besides, a relatively higher graphitic-N content in Co@NC-*800 (al)* (Figure S5d) than in Co@NC-*800* (Figure 3d) is also observed. Taking into consideration that XPS is a surface analysis technique, this is presumably due to more detectable graphitic-N atoms after removal of some cobalt NPs. TEM analysis of acid leached samples reveals that some cobalt NPs together with some hollow carbon shells (Figure 4a) are present in these samples. HR-TEM (Figure S6a) along with H_2 chemisorption results (see experimental section for detail) both demonstrate that the remaining cobalt NPs are tightly encapsulated by multiple graphitic carbon shells which render them inaccessible, even to H_2. Figure 4b shows a high-angle annular dark-field (HAADF) image of the Co@NC-*800 (al)* sample, in which cobalt nanoparticles can be easily distinguished. At the same time, a cloud-like structure dispersed along the carbon support is also noticeable. Although no cobalt nanoparticles can be observed in these regions, cobalt (Figure S6c) is still detected by energy-dispersive X-ray spectroscopy (EDXS) analysis (area 2 in Figure 4b). It has been reported that metal atoms (*e.g.* Co, Fe) released during high-temperature pyrolysis are extremely reactive towards other heteroatoms such as nitrogen to form atomically dispersed metal-N_x species embedded in the carbon matrix.[34] These species, once formed, can be very resistant towards acid leaching. To further demonstrate this claim, we performed additional hydrogenation experiments in the presence of thiocyanate ions (SCN^-), a well-known inhibitor for metal centres in homogeneous catalysts.[35] After the addition of SCN^-, the hydrogenation activity of Co@NC-*800 (al)* decreases from 62% to 39% (Table 1, entry 12). Taking into account that no accessible cobalt NPs are present in the acid leached Co@NC-*800 (al)*, it is proposed that the highly dispersed Co-N_x sites do participate in the hydrogenation process. The reduced activity can be attributed to a competitive adsorption on Co-N_x sites between SCN^- ions and -NO_2 group in nitrobenzene molecules, as it was reported that the thiocyanate does not permanently bind to or alter the metal-centred site but rather interacts competitively.[36] In summary, the superior catalytic activity of Co@NC-*800* can be attributed to the presence of accessible cobalt nanoparticles and atomically dispersed Co in close interaction with the nitrogen doped graphene. Both active species are formed in situ during the pyrolytic transformation of ZIF-67.

A comparison (Table S8) between the *TONs* achieved by the catalysts here reported and literature data reveals that the *TON* value of Co@NC-*900 (al)* obtained for a single run is comparable (*TON* = 101) with the best catalysts reported to date by Beller *et al*. (*TON* = 97)[3a], and larger than those for other Co based catalysts. For repeated runs with Co@NC-*800 and 900(al)*

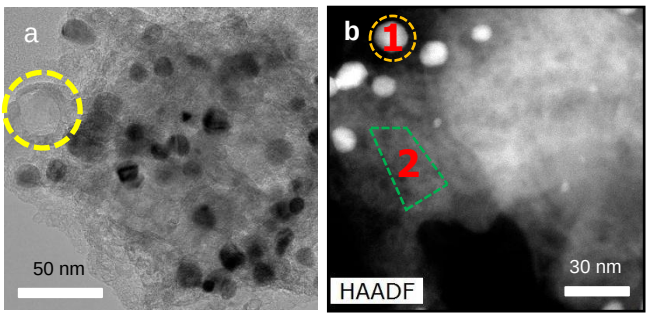

Figure 4. (a) TEM pictures of Co@NC-*800* (*al*), (b) HAADF image of Co@NC-*800* (*al*).

a total *TON* of 118 and 393 is reached (Table S8), respectively (*vide infra*). Furthermore, when productivity is calculated per gram of solid instead of per amount of Co all our catalysts stand out. In view of the characterization performed and the fact that the *TON* doubles already after leaching (Table 1), it is reasonable to argue that the presence of inaccessible, *i.e.* inactive cobalt NPs which are fully encapsulated by the graphite layers, result in lower *TON* values than actually should apply.

Reusability and Catalyst Deactivation

Catalyst stability and reusability is a key factor to evaluate heterogeneous catalysts. In this sense, the most active catalysts, Co@NC-*800* and *900(al)*, were tested in successive runs. The yield of aniline decreases gradually after each run (Fig. 5a and S10), but the aniline selectivity is well preserved in five consecutive runs (> 99%). In spite of this activity decline, after 4 cycles Co@NC-*800* has still half of its activity: extending the reaction time to 12 h leads to an aniline yield as high as 65%. Overall a *TON* of 118 is attained with this catalyst (Table S8). Loss of the active component is one of causes of catalyst deactivation and usually results from leaching in liquid phase reactions. Wei *et al.* observed that 40 *wt.*% of cobalt was lost by the CoO_x@NCNT hybrid after 11 runs in nitrobenzene hydrogenation, and attributed the deactivation to this loss of cobalt.[9a] However, in our case the negligible amount of cobalt found in the solution (< 3 ppm, below the ICP detection limit, Table S7) after each run suggests that the graphite shells prevent leaching of the cobalt NPs under reaction conditions, implying that the observed deactivation cannot be attributed to a loss of cobalt during the hydrogenation. At the same time, both the XRD pattern and C *1s* XPS spectrum of the spent Co@NC-*800* catalyst exhibit the same features as the fresh Co@NC-*800* (Figure S7 and Figure S8), indicative of a well preserved structure after recycling.

TG analysis in air (Figure 5b) indicates a 50 °C lower initial oxidation temperature of the carbon matrix in *fresh* than in *spent* Co@NC-*800*. Bearing in mind that the carbon structure in the fresh and spent Co@NC-*800* is the same, the temperature deviation is ascribed to the number of exposed cobalt sites, considering that oxidized cobalt species can catalyse carbon oxidation at low temperature.[37] For the spent Co@NC-*800* catalyst, a more intense Co *2p* XPS signal from CoO_x is detected compared to the fresh sample (Figure S9). Oxidized cobalt can be *in situ* reduced to its metallic phase by H_2 under similar hydrogenation conditions;[9a, 15] therefore the increase of the CoO_x signal in our case might be attributed to the re-oxidation of cobalt in air after the recycling. A ~3 *wt.*% lower residual mass in the spent Co@NC-*800* than in the fresh catalyst is also observed. As no mass decrease due to possible adsorbed water release is observed below 200 °C, and the delay in the weight loss, the extra ~3 *wt.*% mass loss in Co@NC-*800* (spent) is ascribed to the removal of some strongly adsorbed reaction species (of unknown nature) on the catalyst. Indeed, the presence of strongly adsorbed species would explain the delay in oxidation of carbon support observed in the TGA analysis. Co@NC-*900 (al)* exhibits the highest activity and stability of all samples (Figure S10). The lower content of Co,and the smaller fraction of encapsulated nanoparticles suggest that the highly dispersed Co is associated with the activity in this catalyst system.

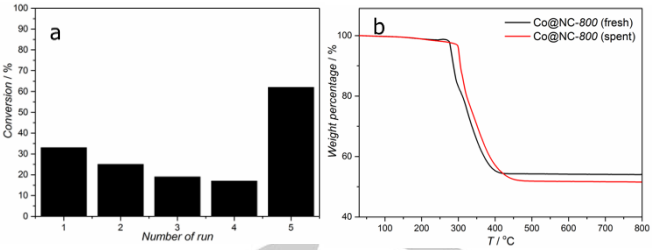

Figure 5. Nitrobenzene conversion upon reuse of Co@NC-*800* (a). Reaction conditions: 3 mmol nitrobenzene, substrate to cobalt molar ratio of 73, 5 mL ethanol, 110 °C, 3 MPa H_2, 3 h for 1st - 4th run and 12 h for the 5th run. (b) TGA curve of Co@NC-*800* (fresh) and Co@NC-*800* (spent) under air flow (100 ml min^{-1} STP, heating rate 5 K min^{-1}).

Hydrogenation of Substituted Nitroarenes

To investigate the general applicability of Co@NC-*800*, various substituted nitroarenes were explored under standard conditions. A variety of industrially relevant anilines such as chloro- and fluoroanilines were produced in high yields and selectivities (Table 2, entries 1-4). The most-challenging substrates bearing other easily reducible groups such as iodides, nitrile, aldehyde, ketone and alkene (Table 2, entries 5-9) could be converted easily and selectively into the corresponding anilines. Even a sterically hindered nitroarene (Table 2, entry 10) was hydrogenated to the substituted aniline with outstanding yield. These results demonstrate again that this Co@NC-*800* catalyst displays an intriguing activity and chemoselectivity in the hydrogenation of substituted aromatic compounds in general.

Conclusions

The one-step thermal decomposition of ZIF-67 under a N_2 atmosphere is a straightforward approach to synthesize a scalable, recyclable and active heterogeneous catalyst for the hydrogenation of nitroarenes. The resulting cobalt containing carbon composites exhibit an excellent catalytic performance in the hydrogenation of a wide range of nitroarenes to their substituted anilines under relatively mild conditions. By controlling the pyrolysis temperature and with a subsequent acid leaching treatment, it is possible to control the total metal loading, resulting in high performance catalysts. The high activity of the Co-N-C system is attributed to cobalt nanoparticles and the presence of highly dispersed Co in close interaction with nitrogen-doped graphene, both of which are formed *in situ* during the pyrolytic transformation of ZIF-67. Furthermore, these atomically dispersed Co-N_x species exhibit a much higher turnover number (*TON*) than cobalt nanoparticles, probably due to its higher cobalt atom utilization in the hydrogenation reaction. Unfortunately, with this MOF-mediated synthesis method, it is

Table 1. Results of the chemoselective hydrogenation of substituted nitroarenes over Co@NC-*800* [a]

Entry	Substrate	Product	t (h)	*Y* (%)[b]
1			4	98
2			6	98
3	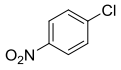	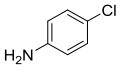	6	97
4	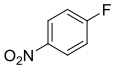	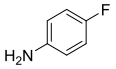	6	97
5			6	97
6	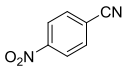	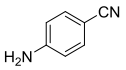	4	96
7[c]			6	96
8	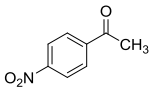	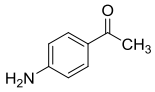	6	98
9[c]	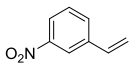	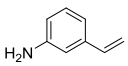	1	47[d]
10			12	99

[a] Reaction conditions: 1 mmol nitroarene, substrate to cobalt molar ratio of 24, 5 mL ethanol, 110 °C, 3 MPa H_2, > 99% conversion observed in all cases. [b] Determined by GC (internal standard: *n*-hexadecane). [c] substrate to cobalt molar ratio of 12. [d] 1 h reaction with 53% conversion. Competing reaction is the double bond hydrogenation[15]

impossible to investigate the differences in N-doped carbon structure and cobalt particle size individually on the hydrogenation performance, and a more in-depth work on these two factors is under investigation. Furthermore, the mild deactivation observed in the Co-N-C catalysts can be attributedto the partial blockage of active sites by strongly adsorbed reaction species.

The presented synthetic approach opens up an avenue to develop and improve powerful non-noble metal catalysts for industrial applications.

Experimental Section

Materials.

2-Methylimidazole (MeIm, purity 99%), cobalt nitrate hexahydrate ($Co(NO_3)_2{\cdot}6H_2O$, >99%), zinc nitrate hexahydrate ($Zn(NO_3)_2{\cdot}6H_2O$, 98%), hydrochloric acid (37%), and methanol (>99.8%) were purchased from Sigma-Aldrich Chemical Co. All chemicals were used without further purification.

Synthesis of ZIF-67 and ZIF-8.

ZIF-67 precursors were synthesized according to a previous report with some modification.[38] Typically, 2.933 g $Co(NO_3)_2{\cdot}6H_2O$ and 6.489 g MeIm were separately dissolved in 200 mL methanol. The clear linker solution was rapidly poured into the metal solution under magnetic stirring and kept at room temperature for 24 h. Afterwards, the bright purple product was collected by filtration, washed 3 times with methanol, and dried at 80 °C under vacuum. For the synthesis of ZIF-8, having the same structure, all the steps are the same except substituting $Co(NO_3)_2{\cdot}6H_2O$ with $Zn(NO_3)_2{\cdot}6H_2O$.

Preparation of Co@NC, Co@NC *(al)* and NC. The Co@NC catalysts were prepared independently but in an almost similar manner as recently reported by Wang and Li[16] Typically, carbonization of 1 g ZIF-67 was performed in a ceramic crucible inside a quartz tubular reactor (approx. *L* = 1.0 m x ID = 5.0 cm) horizontally situated in a ceramic fiber oven (Carbolite, Sheffield). The reactor was flushed with nitrogen (150 ml min^{-1}) at 30 °C for 0.5 h, followed by further carbonization at different temperature for 8 h under N_2 (150 ml min^{-1}) at a ramp of 2 °C min^{-1}. Before exposure to ambient conditions, these catalysts were passivated for 2 h at room temperature in a stream of 5 vol% O_2 in N_2 and denoted herein as Co@NC-*T* (*T* = 600, 700, 800, 900 °C), where *T* refers as the pyrolysis temperature. 0.5 g of the ground Co@NC-*T* samples were further immersed in 200 mL 0.5 M hydrochloric acid solution for 24 h at ambient temperature to dissolve the exposed cobalt nanoparticles. The leaching process was repeated 3 additional times, followed by washing with deionized water until the pH reached ~7. After drying at 50 °C for 24 h under vacuum, these samples are defined as Co@NC-*T (al)* (*T* = 600, 700, 800 °C). For the preparation of NC sample, 1 g ZIF-8 was pyrolyzed at 800 °C followed by a complete acid leaching step with 0.5 M HCl solution, using the same procedures as Co@NC-*800 (al)* sample.

Characterization.

The concentrations of Co and N in the samples were measured by atomic adsorption spectroscopy (AAS) (AAnalyst 200, Perkin Elmer, USA) and elemental analysis (Vario EL, Elementar, Germany), respectively.

The Brunauer-Emmett-Teller (BET) areas and porous structure of the samples were determined using a Micromeritics Tristar 3020 apparatus after degassing under vacuum overnight at 150 °C in Micromeritics Vacprep 061 apparatus.[39]

Thermogravimetric (TG) analysis was carried out using a Mettler Toledo TGA/SDTA851e instrument. The experiments were performed from room temperature to 800 °C with a ramping rate of 5 °C min^{-1} under continuous flow of N_2 or air (100 ml min^{-1}).

Raman spectra were obtained with a commercial Renishaw inVia reflex confocal microscope using a 532 nm laser. Measurements were carried out in samples without any pre-treatment and exposed to normal conditions of air and humidity at room temperature. Spectra analysis was carried with WIRE4.1 software after subtracting the baseline.

X-ray diffraction (XRD) patterns were recorded in Bragg-Brentano geometry in Bruker D8 Advance X-ray diffractometer equipped with a Vantec position sensitive detector and graphite monochromator. Measurements were performed at room temperature with monochromatic Co *Kα* radiation (λ = 0.179026 nm) in the 2θ range (10°-90°).

Transmission electron microscopy (TEM) and high resolution TEM (HR-TEM) images were obtained by using a Talos F200X microscope (FEI, Hillsboro, OR, USA) at 200 kV.

XPS measurements were performed on a *K*-alpha Thermo Fisher Scientific spectrometer using monochromatic Al $K\alpha$ radiation at ambient temperature and chamber pressure of about 10^{-8} mbar. The spot size was 400 µm. A flood gun was always used for charge compensation. All the spectra measured were corrected by setting the reference binding energy of carbon (*1s*) at 284.8 eV. The spectra were analyzed and processed using Thermo Avantage v5.903 software (Thermo Fisher Scientific). The peaks were fitted using Lorentzian–Gaussian product function. Smart background (derived from the Shirley background) was used over the peak width. The binding energy reported is within ± 0.2 eV. H_2 chemisorption was carried out with a Micromeritics ASAP 2020 C instrument using the method reported by Bartholomew and co-workers.[40] Typically, the Co@NC-*800 (al)* sample was first reduced for 3 h in H_2 gas flow at 350 °C, followed by evacuating at that temperature for 30 min. Then, the temperature was cooled down to 150 °C, at which temperature the H_2 adsorption isotherms were measured. The total H_2 uptake at zero pressure was obtained by extrapolating the linear part of the isotherm. The amount of chemisorbed hydrogen is negligible on Co@NC-*800 (al)* sample.

General Procedure for Hydrogenation of Nitroarenes.

The hydrogenation reactions were performed in a Parr 5000 Multi Reactor Stirrer System.[41] The reaction vessels have a volume of 45 cm^3 with stirring and an internal temperature controller. In a typical experiment, hydrogenation reactions are carried out in a batch mode, for which autoclaves are filled with nitrobenzene (1 mmol), an amount of catalyst (Co@NC-*T* or Co@NC-*T (al)*) corresponding to a substrate to cobalt molar ratio of 37 (unless otherwise stated), internal standard (*n*-hexadecane, 0.34 mmol), and 5 ml ethanol as solvent. Before starting the reaction, the autoclaves are purged 3 times with He to remove air, and pressurized to 3 MPa H_2, followed by heating to 110 °C under stirring at 500 rpm. Further increasing stirring speed did not improve the hydrogenation activity. After a fixed reaction time, the autoclaves are cooled down to room temperature and the hydrogen pressure is carefully released. The resulting reaction mixture is filtered and liquids are analyzed by GC (Agilent Technologies, GC 6890N). For recycling studies, 6.5 mg Co@NC-*800* was added into the reactant mixtures (3 mmol nitrobenzene, substrate to cobalt molar ratio of 73, 0.34 mmol *n*-hexadecane, and 5 ml ethanol) under the same conditions as mentioned above except using the recovered catalyst. The catalyst was recovered by filtration, washed three times with ethanol, dried under vacuum at 50 °C for 2 h and then used for the next run without any reactivation or purification.

Acknowledgements

Xiaohui Sun acknowledges support by the China Scholarship Council (CSC). The authors greatly thank Alla Dikhtiarenko for the contribution to the design of the graphical abstract for this paper.

Keywords: nitroarene hydrogenation, chemoselectivity, cobalt, N-doped carbon, deactivation.

[1] aD. Cantillo, M. Baghbanzadeh, C. O. Kappe, *Angewandte Chemie International Edition* **2012**, *51*, 10190-10193; bR. S. Downing, P. J. Kunkeler, H. van Bekkum, *Catalysis Today* **1997**, *37*, 121-136; cN. Ono, *The Nitro Group in Organic Synthesis*, Wiley-VCH, New York, **2001**.

[2] S. Nishimura, *Handbook of Heterogeneous Catalytic Hydrogenation for Organic Synthesis*, Wiley-Interscience, New York, **2001**.

[3] aF. A. Westerhaus, R. V. Jagadeesh, G. Wienhöfer, M.-M. Pohl, J. Radnik, A.-E. Surkus, J. Rabeah, K. Junge, H. Junge, M. Nielsen, A. Brückner, M. Beller, *Nat Chem* **2013**, *5*, 537-543; bA. Corma, P. Serna, *Science* **2006**, *313*, 332-334; cR. V. Jagadeesh, A.-E. Surkus, H. Junge, M.-M. Pohl, J. Radnik, J. Rabeah, H. Huan, V. Schünemann, A. Brückner, M. Beller, *Science* **2013**, *342*, 1073-1076.

[4] aF. L'Eplattenier, P. Matthys, F. Calderazzo, *Inorganic Chemistry* **1970**, *9*, 342-345; bA. Corma, C. González-Arellano, M. Iglesias, F. Sánchez, *Applied Catalysis A: General* **2009**, *356*, 99-102; cH.-U. Blaser, H. Steiner, M. Studer, *ChemCatChem* **2009**, *1*, 210-221; dK. Junge, K. Schroder, M. Beller, *Chemical Communications* **2011**, *47*, 4849-4859.

[5] aG. Vilé, N. Almora-Barrios, N. López, J. Pérez-Ramírez, *ACS Catalysis* **2015**, *5*, 3767-3778; bA. Yarulin, C. Berguerand, I. Yuranov, F. Cárdenas-Lizana, I. Prokopyeva, L. Kiwi-Minsker, *Journal of Catalysis* **2015**, *321*, 7-12; cM. Carrus, M. Fantauzzi, F. Riboni, M. Makosch, A. Rossi, E. Selli, J. A. van Bokhoven, *Applied Catalysis A: General* **2016**, *519*, 130-138.

[6] aA. Corma, P. Serna, P. Concepción, J. J. Calvino, *Journal of the American Chemical Society* **2008**, *130*, 8748-8753; bG. C. Bond, *Chemical Society Reviews* **1991**, *20*, 441-475.

[7] A. M. Tafesh, J. Weiguny, *Chemical Reviews* **1996**, *96*, 2035-2052.

[8] aA. Grirrane, A. Corma, H. García, *Science* **2008**, *322*, 1661-1664; bM. Boronat, P. Concepción, A. Corma, S. González, F. Illas, P. Serna, *Journal of the American Chemical Society* **2007**, *129*, 16230-16237.

[9] aZ. Wei, J. Wang, S. Mao, D. Su, H. Jin, Y. Wang, F. Xu, H. Li, Y. Wang, *ACS Catalysis* **2015**, *5*, 4783-4789; bO. Beswick, I. Yuranov, D. T. L. Alexander, L. Kiwi-Minsker, *Catalysis Today* **2015**, *249*, 45-51; cR. K. Rai, A. Mahata, S. Mukhopadhyay, S. Gupta, P.-Z. Li, K. T. Nguyen, Y. Zhao, B. Pathak, S. K. Singh, *Inorganic Chemistry* **2014**, *53*, 2904-2909.

[10] aL. Zhao, J. Chen, J. Zhang, *Journal of Molecular Catalysis A: Chemical* **2006**, *246*, 140-145; bW. Lin, H. Cheng, J. Ming, Y. Yu, F. Zhao, *Journal of Catalysis* **2012**, *291*, 149-154.

[11] aJ. Lee, O. K. Farha, J. Roberts, K. A. Scheidt, S. T. Nguyen, J. T. Hupp, *Chemical Society Reviews* **2009**, *38*, 1450-1459; bV. K. Mittal, S. Bera, T. Saravanan, S. Sumathi, R. Krishnan, S. Rangarajan, S. Velmurugan, S. V. Narasimhan, *Thin Solid Films* **2009**, *517*, 1672-1676; cB. V. Appa Rao, M. Yakub Iqbal, B. Sreedhar, *Corrosion Science* **2009**, *51*, 1441-1452; dJ. Lee, D. H. K. Jackson, T. Li, R. E. Winans, J. A. Dumesic, T. F. Kuech, G. W. Huber, *Energy & Environmental Science* **2014**, *7*, 1657-1660; eY.-Z. Chen, C. Wang, Z.-Y. Wu, Y. Xiong, Q. Xu, S.-H. Yu, H.-L. Jiang, *Advanced Materials* **2015**, *27*, 5010-5016.

[12] aD. Deng, L. Yu, X. Chen, G. Wang, L. Jin, X. Pan, J. Deng, G. Sun, X. Bao, *Angewandte Chemie International Edition* **2013**, *52*, 371-375; bJ. Deng, P. Ren, D. Deng, L. Yu, F. Yang, X. Bao, *Energy & Environmental Science* **2014**, *7*, 1919-1923; cX. Zheng, J. Deng, N. Wang, D. Deng, W.-H. Zhang, X. Bao, C. Li, *Angewandte Chemie International Edition* **2014**, *53*, 7023-7027.

[13] aL. Zhang, A. Wang, W. Wang, Y. Huang, X. Liu, S. Miao, J. Liu, T. Zhang, *ACS Catalysis* **2015**, *5*, 6563-6572; bY. Hou, Z. Wen, S. Cui, S. Ci, S. Mao, J. Chen, *Advanced Functional Materials* **2015**, *25*, 872-882.

[14] T. Cheng, H. Yu, F. Peng, H. Wang, B. Zhang, D. Su, *Catalysis Science & Technology* **2016**, *6*, 1007-1015.

[15] L. Liu, P. Concepción, A. Corma, *Journal of Catalysis* **2016**, *340*, 1-9.

[16] X. Wang, Y. Li, *Journal of Molecular Catalysis A: Chemical* **2016**, *420*, 56-65.

[17] B. Chen, F. Li, Z. Huang, G. Yuan, *ChemCatChem* **2016**, *8*, 1132-1138.

[18] R. Banerjee, A. Phan, B. Wang, C. Knobler, H. Furukawa, M. O'Keeffe, O. M. Yaghi, *Science* **2008**, *319*, 939-943.

[19] aN. L. Torad, M. Hu, S. Ishihara, H. Sukegawa, A. A. Belik, M. Imura, K. Ariga, Y. Sakka, Y. Yamauchi, *Small* **2014**, *10*, 2096-2107; bS. J. Yang, T. Kim, J. H. Im, Y. S. Kim, K. Lee, H. Jung, C. R. Park, *Chemistry of Materials* **2012**, *24*, 464-470.

[20] J. Tang, R. R. Salunkhe, J. Liu, N. L. Torad, M. Imura, S. Furukawa, Y. Yamauchi, *Journal of the American Chemical Society* **2015**, *137*, 1572-1580.

[21] N. L. Torad, R. R. Salunkhe, Y. Li, H. Hamoudi, M. Imura, Y. Sakka, C.-C. Hu, Y. Yamauchi, *Chemistry – A European Journal* **2014**, *20*, 7895-7900.

[22] S. Gadipelli, T. Zhao, S. A. Shevlin, Z. Guo, *Energy & Environmental Science* **2016**.

[23] B. Y. Xia, Y. Yan, N. Li, H. B. Wu, X. W. Lou, X. Wang, *Nature Energy* **2016**, *1*, 15006.

[24] D. Yang, A. Velamakanni, G. Bozoklu, S. Park, M. Stoller, R. D. Piner, S. Stankovich, I. Jung, D. A. Field, C. A. Ventrice Jr, R. S. Ruoff, *Carbon* **2009**, *47*, 145-152.

[25] aJ. Tang, T. Wang, X. Pan, X. Sun, X. Fan, Y. Guo, H. Xue, J. He, *The Journal of Physical Chemistry C* **2013**, *117*, 16896-16906; bN. A. M. Barakat, B. Kim, S. J. Park, Y. Jo, M.-H. Jung, H. Y. Kim, *Journal of Materials Chemistry* **2009**, *19*, 7371-7378.

[26] Z. Zhuang, S. A. Giles, J. Zheng, G. R. Jenness, S. Caratzoulas, D. G. Vlachos, Y. Yan, *Nature Communications* **2016**, *7*, 10141.

[27] W. Zhou, J. Zhou, Y. Zhou, J. Lu, K. Zhou, L. Yang, Z. Tang, L. Li, S. Chen, *Chemistry of Materials* **2015**, *27*, 2026-2032.

[28] J. R. Pels, F. Kapteijn, J. A. Moulijn, Q. Zhu, K. M. Thomas, *Carbon* **1995**, *33*, 1641-1653.

[29] aJ. Casanovas, J. M. Ricart, J. Rubio, F. Illas, J. M. Jiménez-Mateos, *Journal of the American Chemical Society* **1996**, *118*, 8071-8076; bH.-W. Liang, W. Wei, Z.-S. Wu, X. Feng, K. Müllen, *Journal of the American Chemical Society* **2013**, *135*, 16002-16005; cG. Wu, C. M. Johnston, N. H. Mack, K. Artyushkova, M. Ferrandon, M. Nelson, J. S. Lezama-Pacheco, S. D. Conradson, K. L. More, D. J. Myers, P. Zelenay, *Journal of Materials Chemistry* **2011**, *21*, 11392-11405.

[30] L. Zhang, Z. Su, F. Jiang, L. Yang, J. Qian, Y. Zhou, W. Li, M. Hong, *Nanoscale* **2014**, *6*, 6590-6602.

[31] R. W. Coughlin, *Product R&D* **1969**, *8*, 12-23.

[32] J. Deng, P. Ren, D. Deng, X. Bao, *Angewandte Chemie International Edition* **2015**, *54*, 2100-2104.

[33] aX. Zou, X. Huang, A. Goswami, R. Silva, B. R. Sathe, E. Mikmeková, T. Asefa, *Angewandte Chemie* **2014**, *126*, 4461-4465; bL.-B. Lv, T.-N. Ye, L.-H. Gong, K.-X. Wang, J. Su, X.-H. Li, J.-S. Chen, *Chemistry of Materials* **2015**, *27*, 544-549.

[34] W.-J. Jiang, L. Gu, L. Li, Y. Zhang, X. Zhang, L.-J. Zhang, J.-Q. Wang, J.-S. Hu, Z. Wei, L.-J. Wan, *Journal of the American Chemical Society* **2016**, *138*, 3570-3578.

[35] H.-W. Liang, S. Bruller, R. Dong, J. Zhang, X. Feng, K. Mullen, *Nat Commun* **2015**, *6*.

[36] M. S. Thorum, J. M. Hankett, A. A. Gewirth, *The Journal of Physical Chemistry Letters* **2011**, *2*, 295-298.

[37] J. van Doorn, M. A. Vuurman, P. J. J. Tromp, D. J. Stufkens, J. A. Moulijn, *Fuel Processing Technology* **1990**, *24*, 407-413.

[38] Z. Jiang, Z. Li, Z. Qin, H. Sun, X. Jiao, D. Chen, *Nanoscale* **2013**, *5*, 11770-11775.

[39] M. F. De Lange, T. J. H. Vlugt, J. Gascon, F. Kapteijn, *Microporous and Mesoporous Materials* **2014**, *200*, 199-215.

[40] aR. C. Reuel, C. H. Bartholomew, *Journal of Catalysis* **1984**, *85*, 63-77; bJ. M. Zowtiak, C. H. Bartholomew, *Journal of Catalysis* **1983**, *83*, 107-120.

[41] S. Sartipi, M. J. Valero Romero, E. Rozhko, Z. Que, H. A. Stil, J. de With, F. Kapteijn, J. Gascon, *ChemCatChem* **2015**, *7*, 3243-3247.

Entry for the Table of Contents (Please choose one layout)

Layout 1:

FULL PAPER

Text for Table of Contents

*Author(s), Corresponding Author(s)**

Page No. – Page No.

Title